

Modelling of bonded and unbonded post-tensioned concrete flat slabs under flexural and thermal loading

Abbas H. Mohammed* and Nildem Tayşi^a

Department of Civil Engineering, Gaziantep University, 27310, Gaziantep, Turkey

(Received May 29, 2015, Revised March 1, 2017, Accepted May 11, 2017)

Abstract. During their life span, post-tensioned concrete structures may be exposed to thermal loads. Therefore, there has been a growing interest in research on the advanced analysis and design of post-tensioned concrete slabs subjected to thermal loads. This paper investigates the structural behaviour of post-tensioned one-way spanning concrete slabs. A nonlinear finite element model for the analysis of post-tensioned unbonded and bonded concrete slabs at elevated temperatures was developed. The interface between the tendon and surrounding concrete was also modelled, allowing the tendon to retain its profile shape during the deformation of the slab. The load-deflection behaviour, load-force behaviour in the tendon, and the failure modes are presented. The numerical analysis was conducted by the finite element ANSYS software and was carried out on two different one-way concrete slabs chosen from literature. A parametric study was conducted to investigate the effect of several selected parameters on the overall behavior of post-tensioned one-way concrete slab. These parameters include the effect of tendon bonding, the effect of thermal loading and the effect of tendon profile. Comparison between uniform thermal loading and non-uniform thermal loading showed that restrained post tensioned slab with bottom surface hotter has smaller failure load capacity.

Keywords: post-tensioned slabs; computer modelling; finite element method; concrete; unbonded tendons; bonded tendons; thermal loading

1. Introduction

The Post-Tensioned (PT) slabs commonly used in building and bridge construction are grouped into two basic categories. These are the unbonded and bonded systems. The use of post-tensioning system allows for material savings due to reduced slab thickness. Moreover, cracking and deflection of the concrete slabs can be reduced by using post-tensioning. Post-tensioning of concrete slabs can be conducted using unbonded or bonded tendons. In bonded systems, the tendons are fully bonded to the surrounding material. The tendons are inserted into the ducts and after the pre-stressing load is applied, the ducts are filled with cementitious grout to achieve the required bond between the tendon and the concrete. For bonded systems, there is in principle uniform steel-concrete force transfer along the length of the tendons and full strain compatibility is assumed, implying that steel strains are equal to concrete strains.

For unbonded tendons, each tendon is greased and covered by a plastic tube, as to avoid corrosion and to provide minimum friction between the tendon and the concrete. However, if the tendon is damaged, it will lose all of its pre-stressing at once. For unbonded tendons, steel-concrete force transfer occurs only at the anchors and strain compatibility cannot be assumed at all sections.

The prestressing force that is applied is dependent on the geometry and loading of a specific element and is determined with the principles of mechanics and stress-strain relationships. The prestressing force can be either concentric (along the axis of the member) or eccentric (a distance away from and parallel to the axis of the member). For the concentric case, the compressive stress on the beam cross-section is uniform. The presence of the compressive prestress force reduces the tensile flexural stress at bottom fibers and induces compressive stresses in top fibers. This situation is avoided by applying the prestress force eccentrically. In order to avoid high tensile stresses in the top fiber over the support, tendons are draped or harped over the length of the member.

The behavior of PT concrete structural members have previously been investigated experimentally by Williams and Waldron (1989), Yang *et al.* (2013), Ranzi *et al.* (2013), Bailey and Ellobody (2009a, b) and others. Numerical and theoretical models have been previously developed by other researchers to study the behavior of bonded and unbonded PT concrete members. Kim and Lee (2012) proposed a flexural behavior model for continuous unbonded PT members, which was a nonlinear analysis model that reflects the moment redistribution.

Using the commercial Finite Element (FE) package ANSYS, Fanning (2001) recommended some numerical strategies to model the PT beams without using interface element. Prestressed concrete beams using FE analysis were studied by Kasat and Varghese (2012) to understand the load deflection response and the stress distributions of prestressed concrete beams due to transverse loading. The effect of temperature on the unbonded post-tensioned one-

*Corresponding author, Ph.D. student
E-mail: am20197@mail2.gantep.edu.tr
^aPh.D.

way concrete slabs have been investigated by Ellobody and Bailey (2009a). They developed FE model for the analysis of PT unbonded concrete slabs at raised temperatures.

Ellobody and Bailey (2009a) investigated the structural behaviour of unbonded PT one-way spanning concrete slabs in fire conditions. They developed a nonlinear FE model for the analysis of post-tensioned unbonded concrete slabs at elevated temperatures.

Kang and Huang (2012) using the FE software package ABAQUS to model the PT structures. They used three modelling approaches to simulate bonded and unbonded tendon conditions. The first approach used a multiple-spring system that provides more flexibility in modelling and robustness in convergence issues. The second approach was based on contact techniques, which reflect the true physical condition of the tendon in concrete. The third approach was the simulation using a contact formulation (surface-to-surface contact in ABAQUS/Explicit formulations).

However, FE models studying the behavior of PT concrete one-way slabs under thermal loading have not been adequately developed to date, yet some progress presented by Ellobody and Bailey (2009) using ABAQUS program. Very few researches are presented in literature on the effect of type of support on the behaviour of PT one-way concrete slabs especially the numerical analysis. In addition, modelling of bonded slabs are needed more study especially the modelling of grouting the tendon after applied prestress load. This research presents a FE model using ANSYS software to model the bonded and unbonded PT concrete slabs. The proposed models were validated with previous available experimental study tested by Bailey and Ellobody (2009b) and Yang *et al.* (2013) and was used to study the effects of the transverse, gravity and thermal loading on the flexural behavior of bonded and unbonded PT one-way concrete flat slabs. A thermal version of the model was used to calculate the temperature profile in the concrete slab, following by a structural version of the model, which reads the temperature profile to calculate thermal stresses. A parametric study was conducted to investigate the effect of several selected parameters on the overall behaviour of PT one-way concrete slab. These parameters include the effect of tendon bonding, the effect of thermal loading and the effect of tendon profile.

2. Finite element model

The computer program ANSYS (ANSYS 2012) is used to model and analyze PT concrete one-way slab. SOLID65 (or 3D reinforced concrete solid) (ANSYS 2012) is utilized for 3D modelling of concrete, which is capable of crushing in compression and cracking in tension. The element is modeled by 8-nodes having 3-degrees of freedom at each node.

Tendons and reinforcement were represented using 2-node discrete link elements (LINK8) (ANSYS 2012), which are included within the properties of 8-node brick elements. The link element is assumed to be capable of transmitting only axial forces. For tendon cable, since it is placed inside the slab section (through the hole) and PT force is transferred

to concrete through end anchorages and profile of tendon, the cable is linked to slab only at the end of anchorages. To prevent stress concentration, steel plates were added at location of loading. SOLID45 (ANSYS 2012) is used for 3D modelling of steel plates having 8-nodes with 3-degrees of freedom at each node.

The contact between the concrete and the tendon is modeled by contact elements (using the CONTACT PAIR MANAGER). The method requires the definition of two surfaces that are the target and the contact surfaces. The target surface within this model TARGE170 (ANSYS 2012) represents rigid surface which is defined as the concrete surface surrounding the tendon. The contact surface CONTA175 (ANSYS 2012) represents contact, sliding and deformable surface, which is the tendon surface in this case. This element is located on the surface of a 3D rigid element such as the 8-node brick element and has the same geometric characteristics as the rigid element face with which it is connected. The contact elements are formed using these two elements and monitors the displacement of the contact surface in relation to the target surface. Several contact behaviours are available in ANSYS (ANSYS 2012). For the unbonded tendons the standard behavior was used, while the bonded behaviour was used for bonded tendons.

The tendons must be anchored at both ends of the beam members to maintain the internal forces. These forces create high stresses at both ends. To avoid the ends from crushing the shell plates must be applied at ends. SHELL181 (ANSYS 2012) is suitable for analyzing shell structures. The element is modeled by 4-nodes having 6-degrees of freedom at each node.

Thermal-stress applications are treated in a so-called coupled-field analysis (ANSYS 2012), which consider into account the interaction between thermal expansion/contraction and mechanical stress. The transfer from structural to thermal analysis is done in ANSYS as the elements are switched from SOLID65 structural element to SOLID70 thermal element (ANSYS 2012). The distributions of thermal elastic stress components are then calculated by switching the thermal SOLID70 element to structural SOLID65 element which is used for 3D modelling of solid structures. The FE solution performed via ANSYS calculates nodal temperatures, and then use the nodal temperatures to obtain other thermal quantities. The elastic stresses, induced by thermal strains and mechanical constraints resulting from the previous analysis, are calculated.

Material plays a significant role in ANSYS modelling. Real values of material properties should be given as an input in ANSYS. The stress-strain relationship for concrete in tension is almost linearly elastic up to the maximum tensile strength. Then, the concretes start cracking and the strength decreases continuously to zero. The multi-linear stress-strain relationship is considered for concrete in compression in this study. The adopted stress-strain relation is based on work done by Desayi and Krishnan (1964); as shown in Fig. 1(a). The bilinear stress-strain relationship indicated in Fig. 1(b) is considered for reinforcing steel bars in this study. Since the steel bars are slender, it could be assumed that bars transmit only axial force.

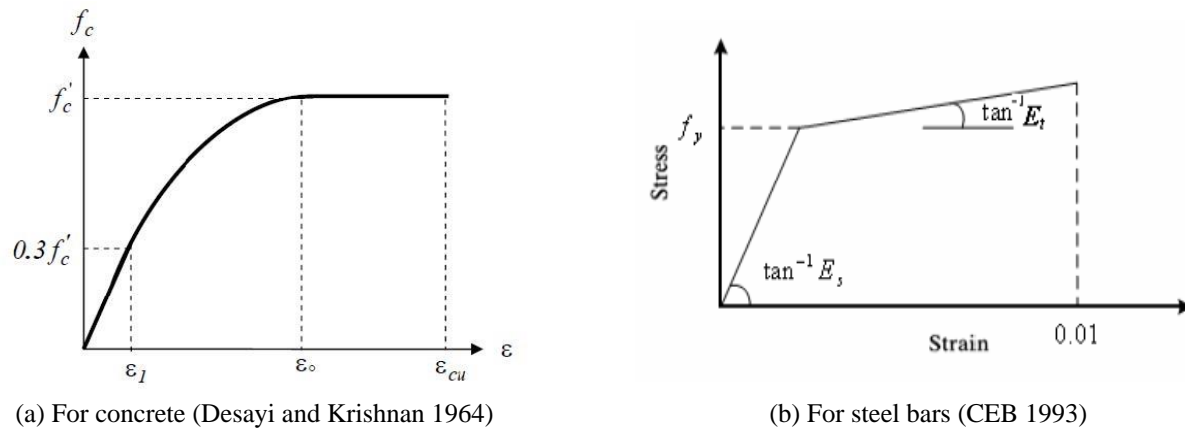


Fig. 1 Stress- strain curve

On the other hand, the strands are considered as multilinear isotropic material in this study.

3. Analysis of post tensioned one-way slabs

3.1 Analysis of unbonded one-way Slab

For the verification of the current numerical model, experimental unbonded post-tensioned concrete slab tested by Yang et al. (2013) was chosen. The slab was designated as 1-H35 with f'_c of 32.64 MPa, which was simply supported and subjected to concentrated point load at the center of the span (Yang et al. 2013).

Fig. 2 illustrates the common layout of the one-way concrete slab PT with unbonded tendons. The tendons producing a prestressing moment reverse to the external moment due to the tendon arrangements with various eccentricity (harped profile). The tendon eccentricities were varied linearly from zero at both ends of the specimens to 37.5 mm at the harping points. The specimen has the section depth of 125 mm and width of 600 mm, as shown in Fig. 2. Two deformed bars with a diameter of 10 mm were used over the full length of the one-way slab and connected to the end anchorage plates. To prevent anchorage failure of the prestressing strands owing to high spalling and bursting stresses the stirrups with diameters of 6 mm were arranged at 50 mm intervals between the ends support. Three-wire strands coated with a greased sheath were arranged for PT tendons. The unbonded tendon was a plain mono-strand with each strand made of three high-strength steel wires. The unbonded tendon had an area of 19.82 mm², a nominal diameter of 2.9 mm.

The equivalent yield strength and tensile strength of the three-wire mono-strand were 1741 MPa and 2048 MPa, respectively. The average density of the concrete mixed was approximately 1770 kg/m³. The yield strengths of the mild reinforcing bars with diameters of 6 mm and 10 mm were 399 MPa and 383 MPa, respectively. The one-way slab was supported on a roller at one end and on a hinge at the other end. Before the test, a designed PT force was applied to tendons and subsequently anchored using a wedge set at both ends of the slab.

The models should mesh for FE analysis as an initial step. The model must be divided into a number of small element, these small element are combined together.

After apply loading, the stresses and strains are calculated at combination points of these small elements (ANSYS 2012). In meshing, the adequate number of elements and mesh density is a very important step to obtain results with high accuracy. To model the concrete, tendon and anchorage elements, the combination of 3D solid elements (SOLID65, LINK8, SHELL181, and SOLID45) was used. These elements have three degrees of freedom for each node. Only one-quarter of the slab was modeled (Fig. 3) due to symmetry, with 14760 elements. The load application and boundary conditions were identical to the tests.

The force in post-tensioning tendons was initially applied in a separate step and equal to (26.38 KN). The weight of slab was applied. The jack load was applied incrementally by way of a distributed load over the area of the spreader plates. The material properties adopted in the analysis are given in Table 1.

The current analysis of a one way slab is a static nonlinear analysis under vertical live, dead and prestress loads. In nonlinear FE analysis, the total load applied to a FE model is divided into a series of load increments called load steps.

The analysis is carried out up to failure, thus it enables determination of failure load. When each load step increments are completed, the stiffness matrix is adjusted to reflect the nonlinear changes in the structural stiffness before the next load increment step is proceeding. For updating the model stiffness ANSYS uses the Newton-Raphson equilibrium iterations.

Convergence criteria were based on displacement are used for the reinforced concrete solid elements, and the convergence tolerance limit is 5% in order to obtain convergence of the solutions. The load increment increase up to a maximum load step size if the convergence behaviour is smooth and the load increment bisect until it is equal to a minimum load step size if the convergence behaviour is abrupt.

The load-central deflection curves from the FE analysis were compared with those from the experimental results.

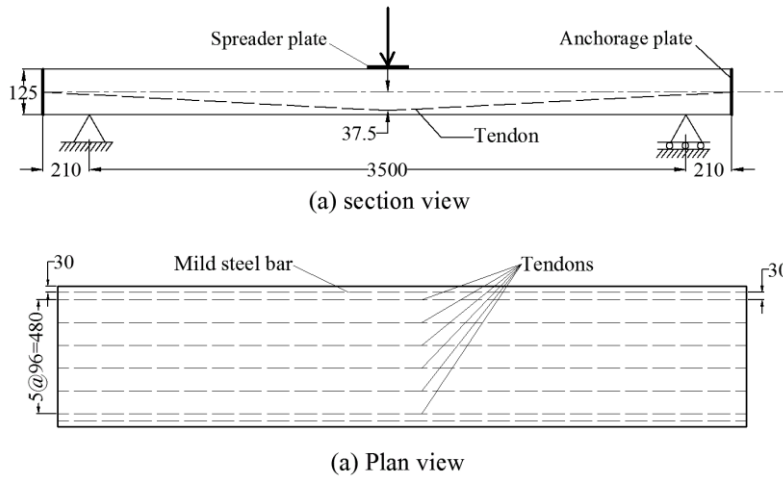


Fig. 2 Details of slab geometry and arrangement of reinforcement of unbonded slab 1-H35 (Yang *et al.* 2013) (dimensions are in mm)

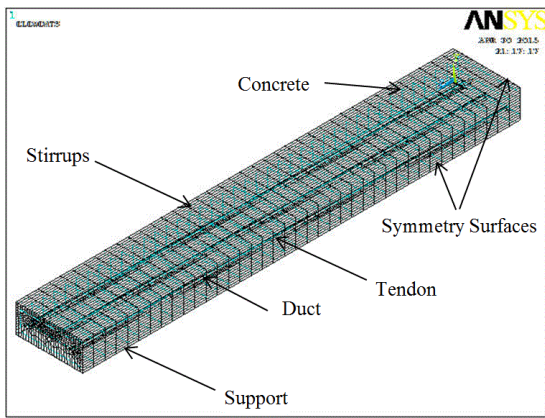


Fig. 3 Finite element mesh of the concrete and the prestress strand for quarter of the unbonded slab 1-H35

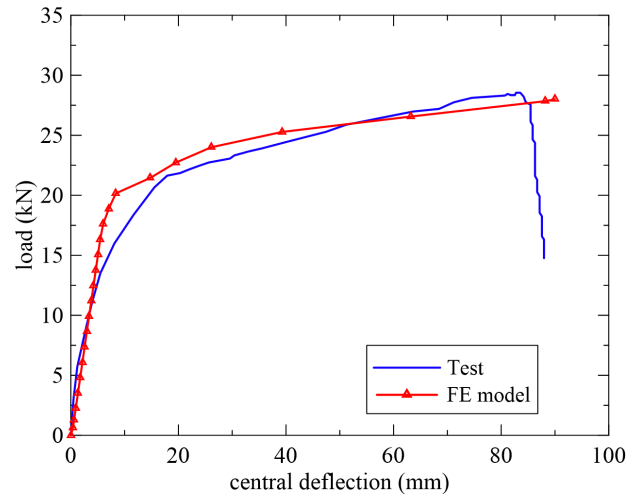


Fig. 4 Load- deflection curve for the unbonded slab 1-H35

Table 1 Material properties of concrete, reinforcement and strand for the unbonded slab

	Concrete	Reinforcement		Strand
		10 mm	6 mm	
Ultimate compressive strength (MPa) (f'_c)	32.64	—	—	—
Ultimate tensile strength (MPa) (f_t)	3.2	—	—	—
Modulus of elasticity (MPa)	30000	205000	204000	202000
Poisson's ratio (ν)	0.2	0.3	0.3	0.3
Yield strength (MPa)	—	383	399	1741

The experimental and numerical load deflection curves obtained for slab 1-H35 are shown in Fig. 4, which shows the good agreement between the experimental and the FE results.

At ultimate state, the numerical load was slightly smaller than the experimental load. The failure load of the experimental slab was 28.5 kN with a central deflection of 83.5 mm, compared to 28 kN and 90 mm obtained from the

FE model. The failure load predicted using the model was 1.8% smaller than that observed from the test. The mode of failure in the FE analysis was concrete crushing corresponded to the mode of failure in experimental. The first flexural cracking was initiated at 71% of the ultimate load and was observed in the tension zone of the slab.

3.2 Analysis of bonded one-way slab

The behaviour of bonded PT concrete slabs is more complicated by reason the presence of ducts, the bond between concretes and ducts, the bond between ducts and grout, and the bond between grout and tendons.

Two stages of analysis are needed for bonded slabs. At the first stage the slab is analyzed as unbonded PT slab under prestress loading and gravity loading only. Next the slab is analyzed as bonded post tensioned slab. The two stages are needed because the grout is added after the prestressing of the strands.

Bonded PT concrete slab (TB2) tested by Bailey and Ellobody (2009b) was chosen for numerical analyses verification. The designated compressive strength of the

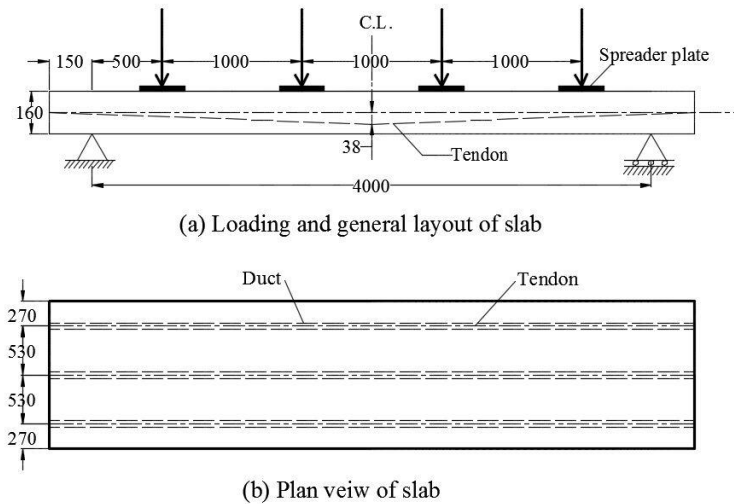


Fig. 5 Details of bonded slab geometry and loading TB2 (Bailey and Ellobody 2009b) (dimensions are in mm)

used concrete was 30.3 MPa. The slab was simply supported at both ends and subjected to four concentrated point loads. PT slab was designed according to BS8110-1. The general layout of the bonded PT one-way concrete is shown in Fig. 5(a). The tendons were a plain mono-strand with each strand made of seven high-strength steel wires. The tendons had a measured tensile strength of 1846 MPa, diameter of 15.7 mm and area of 150 mm². The load was applied gradually in equal increments of 5 kN. Three longitudinal ducts have been used in the slab (one in the middle and the other two were on both sides, at a spacing of 530 mm) as illustrated in Fig. 5(b). At the middle of the slab height, the duct ends were fixed. The strength of grout was 47 MPa after 28 days. The full applied design PT force to the one-way slabs was 195 kN, with the measured force in the tendon being 169 kN, equating to 13% losses (Bailey and Ellobody 2009b). The slabs were tested over a total span length of 4.0 m.

In this paper, the bonded PT concrete slab was modeled using 3D solid elements available within ANSYS (ANSYS 2012). Because of symmetry, only one-quarter of the slab was modelled with 11100 elements, including the contact elements. Load applications and boundary conditions were the same as that utilized in the test. The measured post-tensioning force in the tendons (169 kN) was initially applied in a separate step. The weight of the slab was applied as a static body load.

Bailey and Ellobody (2009b) observed that there was no slip at the interface between the grout and duct as well as at the interface between the duct and concrete. Hence, only the interface between the grout and tendon was modelled utilizing contact elements (using the contact pair option) available within the ANSYS element library. The interface elements composed of two contact surfaces from the tendon elements and surrounding grout elements. The designed tendon axis distance (i.e., at the centre of the duct) will be used in the FE analysis for slab TB2.

The FE mesh of the concrete and the PT strand for quarter of the slab TB2 is shown in Fig. 6. The material properties adopted in the analysis are given in Table 2.

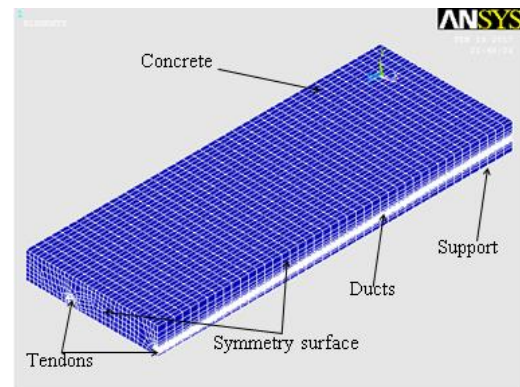


Fig. 6 Finite element mesh of the concrete and the prestress strand for quarter of the bonded PT slab TB2

Table 2 Material properties of concrete, reinforcement and strand for the bonded slab

	Concrete	Steel plate	Strand
Ultimate compressive strength (MPa) (f'_c)	30.3	—	—
Ultimate tensile strength (MPa) (f_t)	3.0	—	—
Modulus of elasticity (MPa)	30000	200000	202000
Poisson's ratio (ν)	0.2	0.3	0.3
Yield strength (MPa)	—	400	1846

The results observed from the FE model in terms of the ultimate loads and load-central deflection curves were compared against the test results (Bailey and Ellobody 2009b). Fig. 7 represents the load-deflection curve obtained from FE analysis and experimental results for the slab TB2, and good agreement can be noticed from the figure. The failure load and central deflection obtained from the experiment were 187.9 kN and 107 mm respectively, while the failure load and central deflection obtained from FE analysis were 186 kN and 117 mm respectively. The failure load predicted from FE analysis was 1.06% less than that obtained from the experiment.

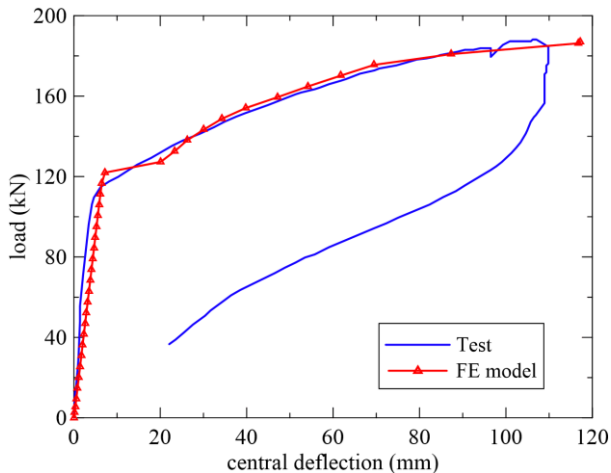


Fig. 7 Load- deflection curve for the bonded slab TB2

The deformed shape at failure for slab TB2, obtained from the model, is shown in Fig. 8(a). The stress (Z-direction) distribution in the concrete at failure is shown in Fig. 8(b).

The type of failure of concrete crushing in this model, which corresponded to the type of failure noticed experimentally and reported by Ellobody and Bailey (2009b).

The strains in the concrete elements in the mid-span near the maximum compressive strains. Hence the local concrete crushing was expected using the FE model, which compares well with the behaviour noticed in the experimental slab (Bailey and Ellobody 2009b).

4. Parametric studies and discussions

The verified FE model was used to investigate the effect of several selected parameters on the overall behaviour of PT one-way concrete slabs. These parameters include the effect of tendon bonding, the effect of thermal loading and the effect of tendon profile. For the proposed study, slab TB2 is chosen. The loading, geometry and boundary conditions considered for the proposed study for slab TB2 are shown in Fig. 9.

The material properties adopted in the proposed study are given in Table 2. The different parameters considered in the parametric study are divided in five groups. Group G1 included four slabs that used to study the effect of bonding. Groups G2 and G3 were subjected to thermal loading. To study the effect of tendon profile, four different tendon profiles are included in groups G4 and G5.

Group G1 included four slabs S1-S4 that used to study the effect of bonding. The load-deflection responses for both bonded slabs S1-S2 and unbonded slabs S3-S4, from the FE analysis, are plotted in Fig. 10. It was observed that the ultimate load capacity for the slabs with bonded tendon are 9.4 and 10.5% higher than the slabs with unbonded tendon for the simply and fix supported slabs respectively. The higher ultimate capacity for bonded slab is due to additive stiffness comes from bonding with concrete. It is clear from the FE analysis that the response of the slabs is

linear until the first crack has formed at approximately 62 and 83 kN for the simply and fix supported slabs respectively.

The ultimate central deflection of the bonded and unbonded slabs were 52.2 mm and 41.4 mm respectively for the simply supported slabs. From Fig. 10(a), it can be shown that the deflection of the unbonded slab is greater than the deflection of bonded slab at the same load after the cracking, which means that the stiffness of bonded slab is greater than the stiffness of the unbonded slab after cracking.

Fig. 11(a) shows that the maximum tensile stress in concrete at the bottom fiber of the center of the bonded slab is greater than that of the unbonded simply supported slab and due to fixity of support, Fig. 11(b) shows the inverse. At higher loads, and due to the presence of the crack, the stress becomes zero or near the zero.

The forces in post tensioned tendons for both bonded and unbonded tendons are shown in Fig. 12. From the figure it can be found that the force in the bonded tendons is higher than the force in unbonded tendons in the center of the slab, while the opposite stands at the support. Note that the force in the unbonded tendon does not change along the slab.

The effect of the thermal loading was investigated by modelling twelve slabs S5-S16. The groups of slabs are denoted as G2 and G3. Three types of thermal load are applied. The three types of thermal load are top surface hotter, bottom surface hotter and uniform temperature. In the top surface hotter, a temperature of 65°C is applied in the top of the slab and 15°C is applied on the bottom of the slab, while the bottom surface hotter case is the inverse. In the uniform temperature, a temperature of 65°C is applied uniformly to slab as shown in Fig. 13. The concrete initial temperature is set to 15°C.

The slab is analyzed under the effect of change in temperature together with the prestress, self-weight and live loading. The slabs are loaded under all loading to the failure. The effect of thermal loading was also applied on the tendon. The thermal load was applied as an initial strain to tendon elements. The thermal strain decreases the total prestressing force of tendons if change in temperature is positive and the inverse is right.

The free and restrained slabs were modelled as the simply and fixed support slab respectively. We have used the free and restrained terms because we are dealing with thermal load.

The plots of load versus central deflection are displayed in Fig. 14. For the restrained bonded slab, the failure loads were 261 kN, 227 kN and 187 kN for uniform, top surface hotter and bottom surface hotter cases respectively. On the other hand, for restrained unbonded slab, the failure loads were 284 kN, 216 kN and 186 kN for top surface hotter, uniform and bottom surface hotter cases respectively. From this figure it can be seen that the failure load capacity for restrained post tensioned slab with bottom surface hotter load is the lowest due to the effect of thermal strain. The thermal strain coming from bottom surface hotter load causes tensile stress at top and compressive stress at bottom, which is the opposite sign with prestress stresses, hence it

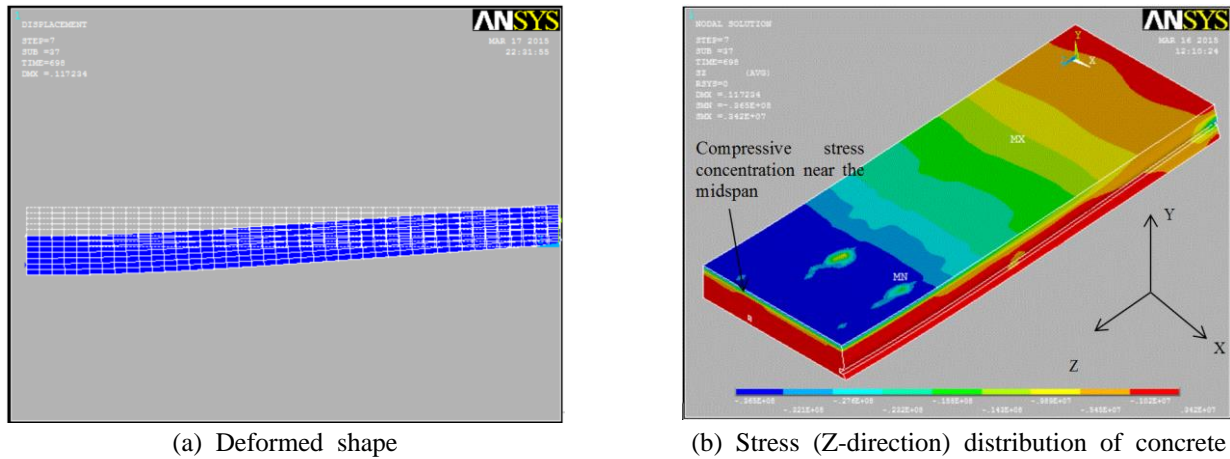


Fig. 8 FE results for the bonded slab TB2

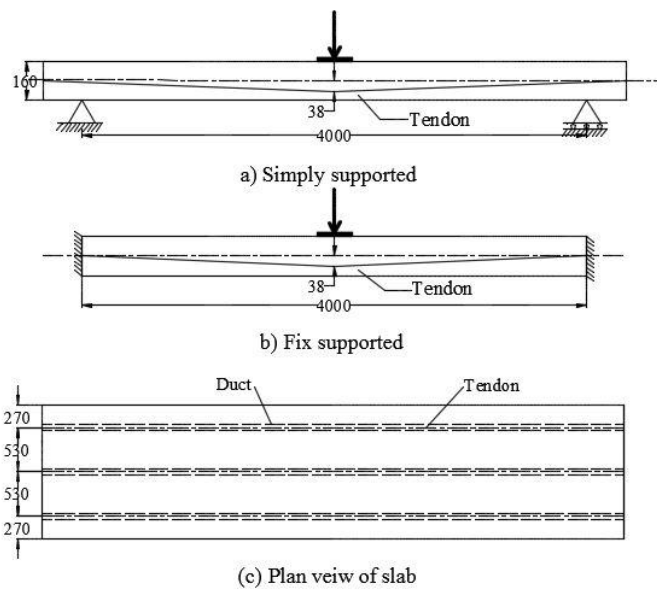


Fig. 9 Loading, geometry and boundary conditions of the TB2 slab for the parametric study

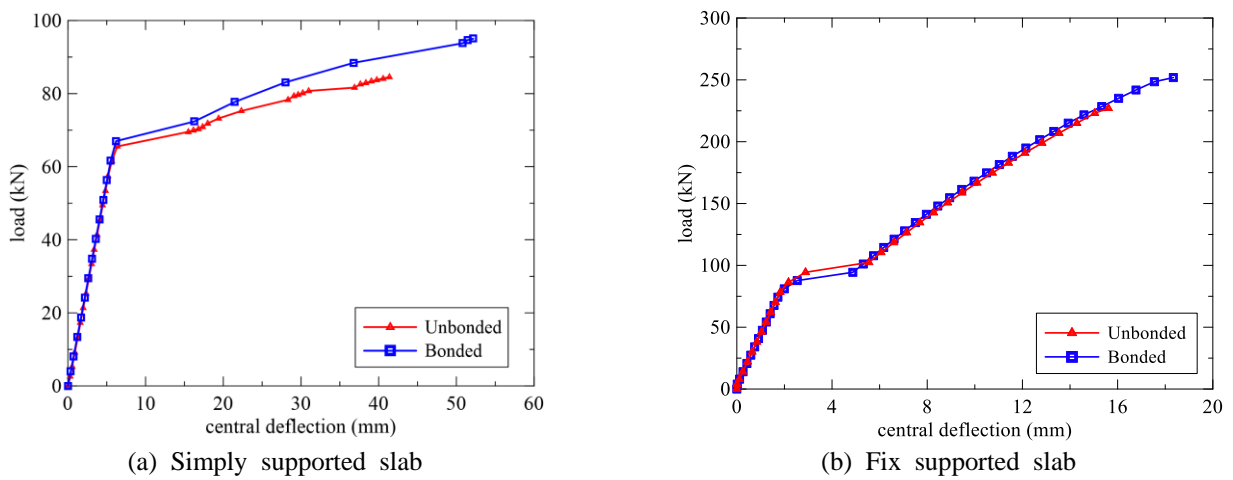


Fig. 10 Effect of bonding on ultimate failure load

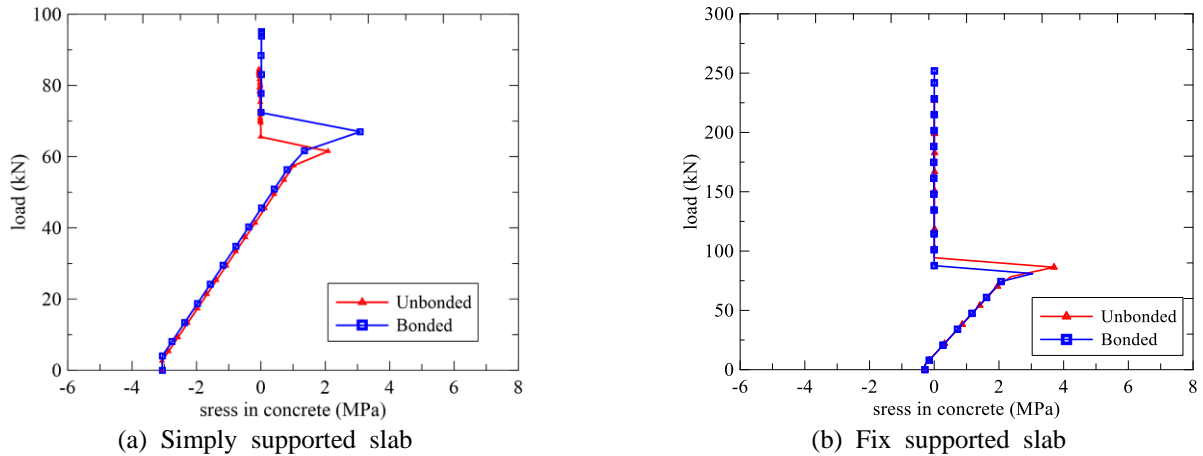


Fig. 11 Effect of bonding on concrete stress of the bottom fiber at center of the slab

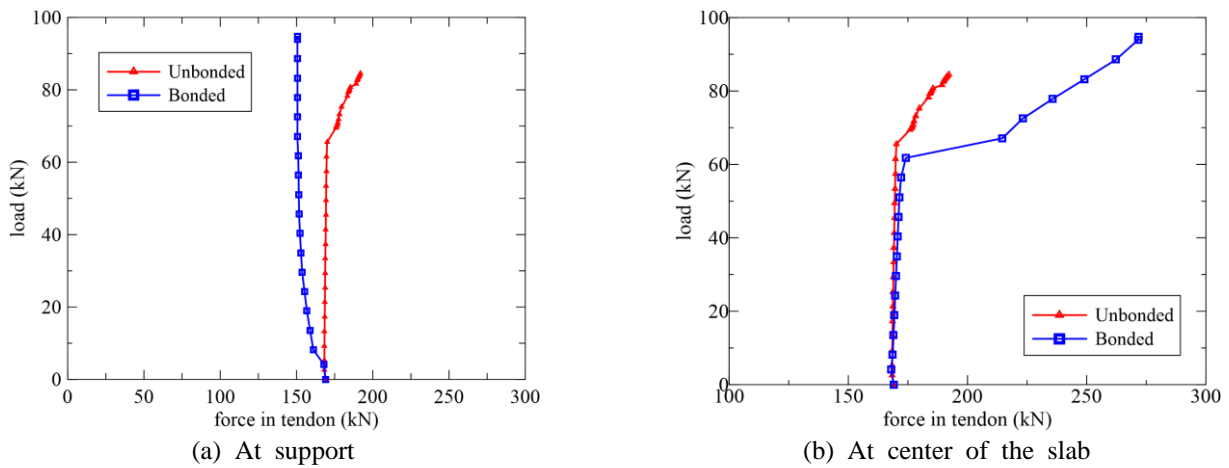


Fig. 12 Effect of bonding on tendons force for the simply supported slab

Table 3 Stresses in the top and bottom fiber at center of proposed slab

	Stress in the top fiber (MPa)				Stress in the bottom fiber (MPa)			
	Bonded slab		Unbonded slab		Bonded slab		Unbonded slab	
	Restrained	Free	Restrained	Free	Restrained	Free	Restrained	Free
Due to prestress and self-weight only	0.24	-1.1	0.17	-1.2	-3.5	-3.1	-3.4	-3.1
Top surface hotter	-20.4	-1.8	-20.1	-1.9	-3.1	-4.0	-10.5	-3.5
Bottom surface hotter	0.84	-0.87	0.84	-0.9	-16.0	-2.8	-16.0	-2.7
Uniform temperature	-19.3	-0.17	-18.4	0.08	-19.4	-4.3	-16.8	-4.5

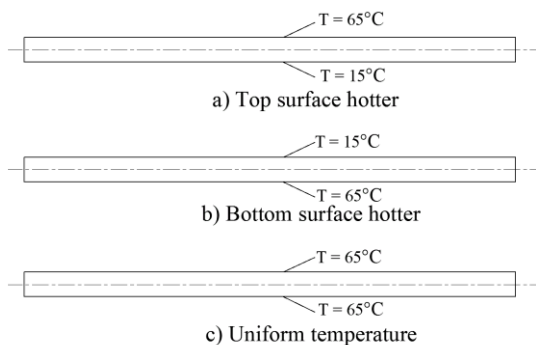
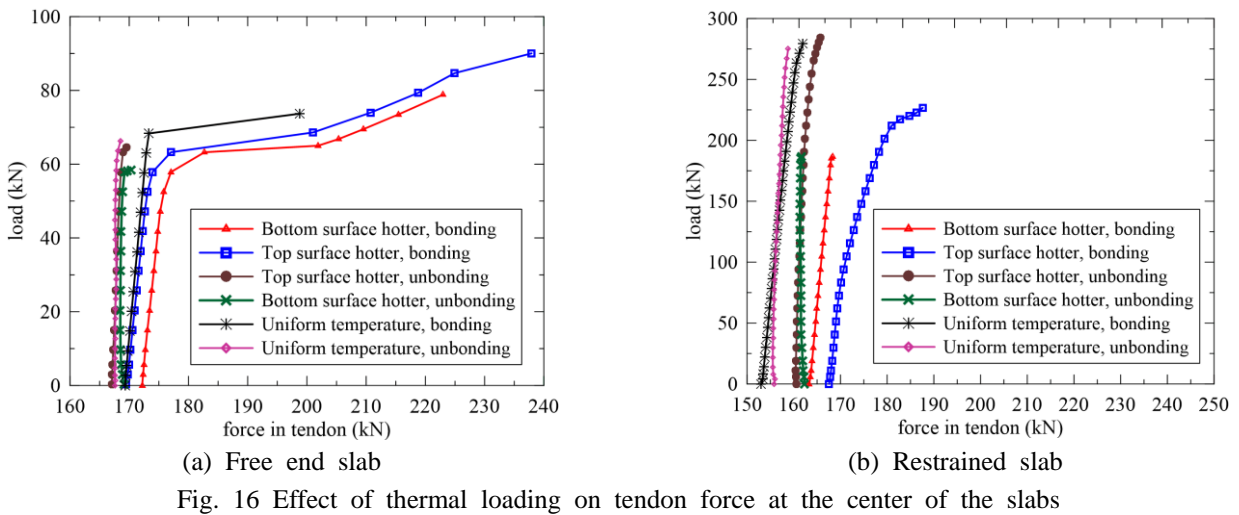
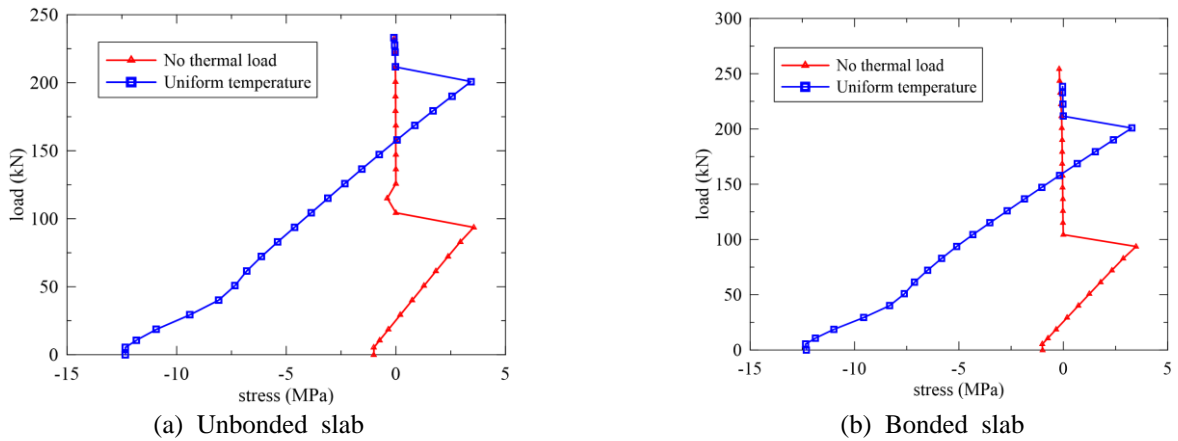
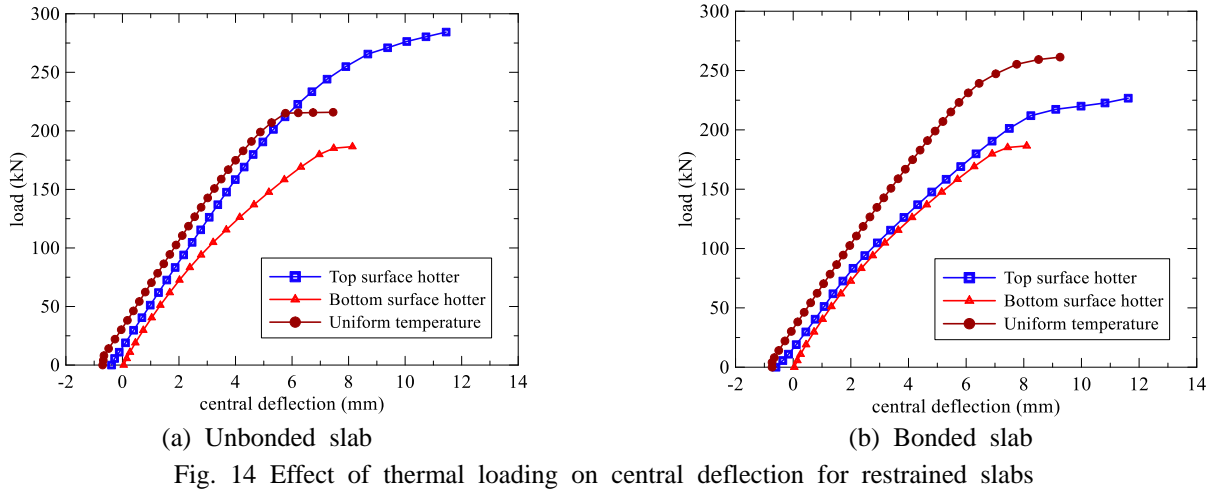


Fig. 13 Thermal loading applied to proposed slabs

decreases the prestress stresses. From Fig. 14, it is also obvious that the failure load capacity of restraint unbonded slab is greater than the failure load capacity of restraint bonded slab under the same top surface hotter load. The higher failure load capacity is due to the higher compressive stress in the bottom fiber for unbonded slab as shown in Table 3.

From Table 3, it can be seen that the compressive stresses in the bottom fiber were 3.1 MPa and 10.5 MPa for bonded and unbonded restrained slabs, respectively.

Fig. 15 shows the load-stress curves of concrete at the bottom fiber of the mid-span the restrained slabs. The stress



increases proportionally with loading until the crack or the crash occurs. After that, the stress decreases rapidly downward to zero value and continues with an approximately constant value near the zero. Zero values mean that the concrete is cracked at this fiber or at least the element beside this element is cracked. The figure shows that the stresses start with compressive stress due the effect

of the positive temperature strain. The compressive stress occurs only in constrained slab.

From Fig. 16 it can be observed that losses in prestress force in restrained slab are the smallest when the slab is bonded and subjected to top surface hotter load, while the losses are the highest when the slab is bonded and subjected to uniform temperature load. The losses in tendon force

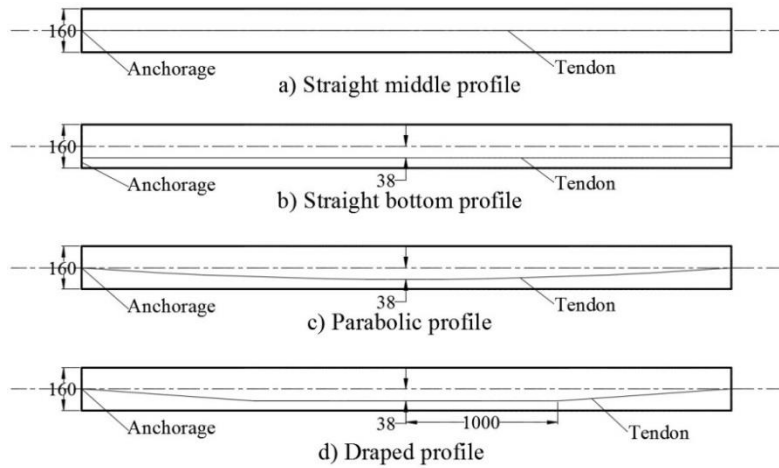


Fig. 17 Proposed tendons profiles

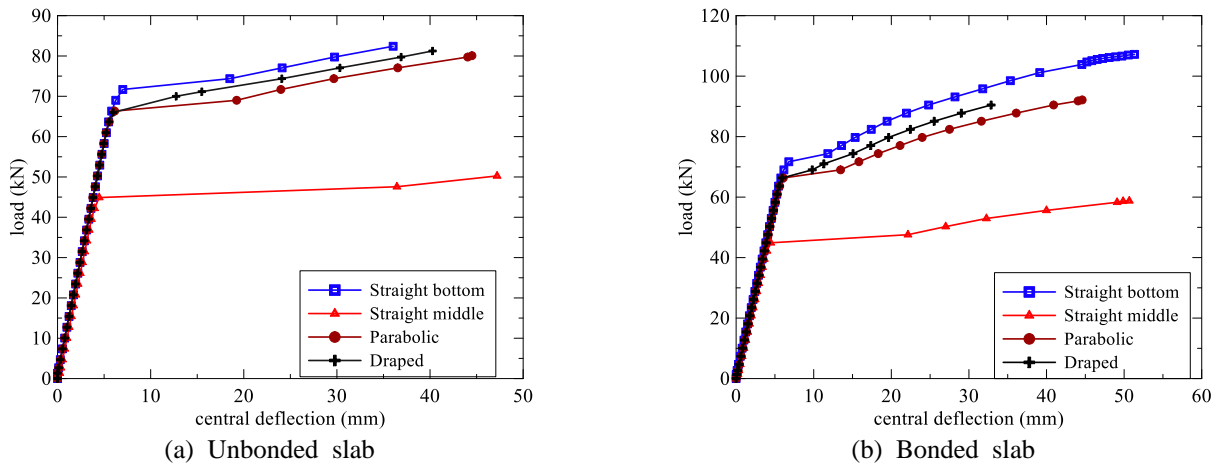


Fig. 18 Effect of tendon profile on central deflection for simply supported slab

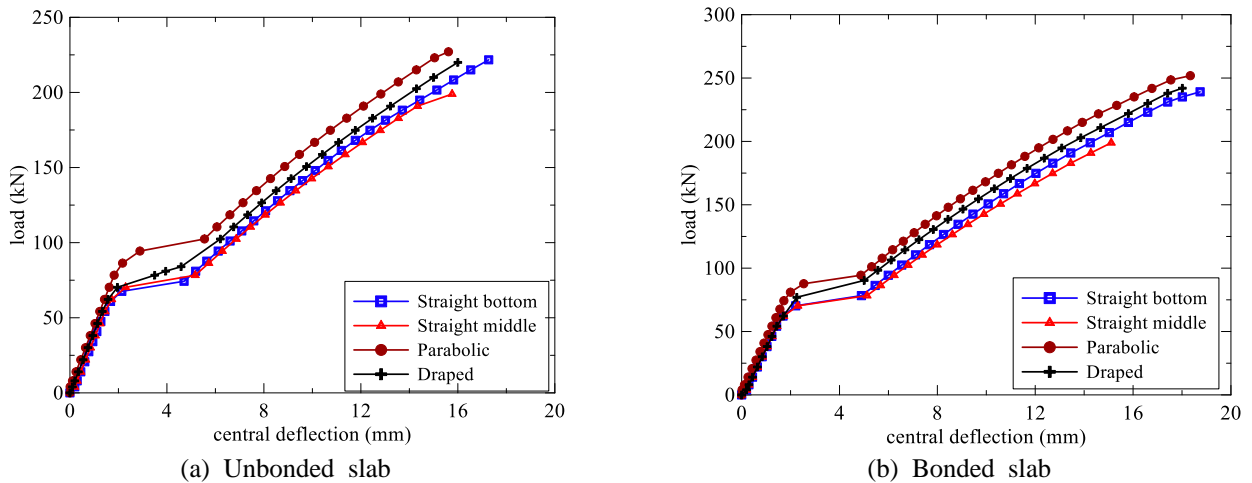


Fig. 19 Effect of tendon profile on central deflection for fix supported slab

occur due to the increase in compressive stress at the bottom fiber and especially in restrained slab. From Table 3, it can be noted that the lowest compressive stress at the bottom fiber is 3.1 MPa for bonded restrained slab with top surface hotter loading, while the highest compressive stress

at the bottom fiber is 19.4 MPa for bonded restrained slab with uniform temperature loading.

The effect of the tendons profile was investigated by modelling sixteen slabs S17-S32. The groups of slabs are denoted as G4 and G5. Four types of tendons profiles are

Table 4 Summary of the parametric study results

Group	Slab	Type of slab	Type of support	Tendon profile	Thermal loading	Longitudinal expansion	Max. deflection (mm)	Failure load (kN)	Max. force in tendon (kN)	
G1	S1	Bonded	Simply	Parabolic	No thermal load	Free	52.2	93.0	272.5	
	S2		Fixed				18.9	251.0	198.8	
	S3	Unbonded	Simply				41.4	85.0	192.1	
	S4		Fixed				15.3	227.2	178.2	
G2	S5	Bonded	Fixed	Parabolic	Top hotter	Restraint	11.6	227.0	187.1	
	S6				Bottom hotter		8.1	187.0	168.4	
	S7		Uniform		9.3		261.3	161.9		
	S8		Top hotter		28.0		91.0	237.9		
	S9		Simply		Bottom hotter		Free	28.8	78.9	222.9
	S10		Uniform		7.0		73.7	198.8		
G3	S11	Unbonded	Fixed	Parabolic	Top hotter	Restraint	11.5	284.3	165.7	
	S12				Bottom hotter		8.1	186.5	161.6	
	S13		Uniform		7.5		216.0	158.8		
	S14		Top hotter		1.1		64.0	169.5		
	S15		Simply		Bottom hotter		Free	13.3	58.4	170.3
	S16		Uniform		4.5		66.3	168.5		
G4	S17	Bonded	Simply	Straight Bottom	No thermal load	Free	51.3	107.2	269.1	
	S18		Fixed				18.7	239.1	206.6	
	S19		Simply	Parabolic			44.6	92.1	270.8	
	S20		Fixed				18.3	251.8	198.2	
	S21		Simply	Straight Middle			50.7	58.8	242.8	
	S22		Fixed				15.1	199.0	182.2	
	S23		Simply	Draped			32.8	90.5	183.5	
	S24		Fixed				17.9	242.3	199.1	
G5	S25	Unbonded	Simply	Straight Bottom	No thermal load	Free	36.0	82.4	195.4	
	S26		Fixed				17.3	221.7	174.2	
	S27		Simply	Parabolic			44.5	80.1	199.1	
	S28		Fixed				15.6	227.0	178.2	
	S29		Simply	Straight Middle			47.2	50.3	189.0	
	S30		Fixed				15.8	199.0	174.2	
	S31		Simply	Draped			40.2	81.2	175.1	
	S32		Fixed				16.1	220.3	174.5	

considered. These are the parabolic, the straight at middle, the straight at bottom and draped profiles as shown in Fig. 17. The central deflection for the four profiles are plotted in Figs. 18-19. It is noted the straight bottom profile has the highest load capacity for the simply supported post tensioned slab. For the fixed post tensioned slab, the

parabolic profile resulted in the maximum load capacity. Comparison between the simply supported slab and the fixed slab shows that the slab with fix ends has the largest percentage of failure load to first cracking load (Figs. 18-19).

From Fig. 18, It can be found that the tendon profile has

a significantly effect on the ultimate load capacity, where the results showed that ultimate load increased 81 and 64% with straight bottom tendon profile compared to straight middle tendon profile for the bonded and unbonded simply supported slab respectively.

The different parameters considered in the parametric study and their results are summarized in Table 4. The values presented in this table are the maximum values from the result analysis of all slabs. From Table 4, it can be shown that the failure loads for the restrained slabs are greater than for the free end slabs. The higher ultimate capacity for restrained slabs are due to fixed support. In addition, thermal expansion in restrained slabs generates compressive stresses in the longitudinal direction that, as a result, decrease tensile stresses in the slab. Tensile stresses play a major role in the ultimate capacity of the concrete structures.

In addition, it can be noted that for groups G2 and G3 the unbonded restrained slab with top hotter (S11) has the highest failure load (284.3 kN), while the highest deflection (28.8 mm) occurs in bonded free slab with bottom hotter (S9). For groups G4 and G5, it was found that the bonded simply supported slab with a straight bottom profile (S17) has the highest deflection (51.3 mm). The highest tendon force (272.5 kN) occurs in center of simply supported bonded slab (S1).

5. Conclusions

In this paper, a 3D thermo-mechanical nonlinear FE model is developed to study the behavior of bonded and unbonded PT concrete slabs. The contact between the concrete and the tendon is modeled by contact elements. Contact elements allowing the post-tensioned tendon to retain its profile during the deformation of the slab and modelling the bond behaviour between the grout and tendon.

Experimental bonded and unbonded PT concrete one-way slabs from literature were chosen for numerical analyses verification, and good agreement was achieved between numerical and test results.

This study investigates the effect of several factors on the load-deflection response throughout the entire range of behavior using the nonlinear analysis of the ANSYS FE program. The verified finite element model was used to investigate the effect of several selected parameters on the overall behavior of PT one-way concrete slab. These parameters include the effect of tendon bonding, the effect of thermal loading and the effect of tendon profile.

It was observed that the ultimate load capacity for slab with a bonded tendon increased by 9 % compared to the same slab with unbonded tendon. The higher ultimate capacity for bonded slab is due to the additive stiffness obtained by tendon-concrete bond. The force in bonded tendon is higher than the force in unbonded tendon in the center of the slab, while the opposite stands at the support.

The flexural behaviour of one way PT slab due to thermal loading is studied by applying three types of thermal load. The three types of thermal load are top surface hotter, bottom surface hotter and uniform

temperature. It was found that the failure loads for the restrained slabs are greater than free end slabs. It was observed, for restrained slabs, that the failure load capacity for slab with bottom surface hotter load is the smallest due to the effect of thermal strain. The thermal strain coming from the bottom surface hotter load causes tensile stress at top and high compressive stress at the bottom which is the in the opposite sign with prestress stress, and hence decreases the prestress stress. It is also shown that losses in prestress force on restrained slab is smaller when the slab is bonded and subjected to top surface hotter load, while the losses is higher when the slab is bonded and subjected to uniform temperature load. The losses in tendon force occur due to increase in compressive stress at bottom fiber and especially for restrained slab. For free slabs, it was found also that the failure load capacity for slab with bottom surface hotter load is the smallest.

For the effect of profile, it was observed that the straight bottom profile resulted in the maximum load capacity for the simply supported post tensioned slab. For the fixed end post tensioned slab, the parabolic profile showed the maximum load capacity.

References

- ANSYS (2012), *ANSYS Help*, Release 14.5, Copyright.
- Bailey, C.G. and Ellobody, E. (2009a), "Fire tests on unbonded post-tensioned one-way concrete slabs", *Magaz. Concrete Res.*, **61**(1), 67-76
- Bailey, C.G. and Ellobody, E. (2009b), "Fire tests on bonded post-tensioned concrete slabs", *Eng. Struct.*, **31**(3), 686-696.
- Ellobody, E. and Bailey, C.G. (2009), "Modelling of unbonded post-tensioned concrete slabs under fire conditions", *Fire Safe. J.*, **44**(2), 159-167.
- European Committee for Standardization (CEB), Eurocode 3, (1993), Design of Steel Structures. Part 1.1: General Rules and Rules for Buildings, DD ENV, 1-1, EC3.
- Desayi, P. and Krishnan, S. (1964), "Equation for the stress-strain curve of concrete", *J. Am. Concrete Inst.*, **61**(3), 345-350.
- Fanning, P. (2001), "Nonlinear models of reinforced and post-tensioned concrete beams", *Electronic J. Struct. Eng.*, **2**, 111-119.
- Kang, T. and Huang, Y. (2012), "Computer Modeling of Post-Tensioned Structures", *4th International Conference on Computer Modeling and Simulation (ICCMS 2012)*, Singapore.
- Kasat, A.S. and Varghese, V. (2012), "Finite element analysis of prestressed concrete beams", *Int. J. Adv. Technol. Civ. Eng.*, **1**(3, 4), 2231-5721.
- Kim, K.S. and Lee, D.H. (2012), "Nonlinear analysis method for continuous post-tensioned concrete members with unbonded tendons", *Eng. Struct.*, **40**, 487-500.
- Ranzi, G., Al-Deen, S., Ambrogi, L. and Uym, B. (2013), "Long-term behaviour of simply-supported post-tensioned composite slabs", *J. Constr. Steel Res.*, **88**, 172-180.
- Williams, M.S. and Waldron, P. (1989), "Movement of unbonded post-tensioning tendons during demolition", *Proceedings of the Institution of Civil Engineers*, Part 2, **87**, 225-253.
- Yang, K.H., Mun, J.H. and Kim, G.H. (2013), "Flexural behavior of post-tensioned normal-strength lightweight concrete one-way slabs", *Eng. Struct.*, **56**, 1295-1307.